Human immunodeficiency virus type 2 capsid protein mutagenesis defines the determinants for Gag – Gag interactions

Huixin Yang[1,4], Nathaniel Talledge[1,2,3], William G. Arndt[1,2,5], Wei Zhang[1,2,6]* and Louis M. Mansky[1,2,3,4,5,6]*

[1] Institute for Molecular Virology, University of Minnesota – Twin Cities, Minneapolis, MN 55455 USA

[2] Division of Basic Sciences, School of Dentistry, University of Minnesota – Twin Cities, Minneapolis, MN 55455 USA

[3] Masonic Cancer Center, University of Minnesota – Twin Cities, Minneapolis, MN 55455 USA

[4] Comparative Molecular Biosciences Graduate Program, University of Minnesota – Twin Cities, St. Paul, MN 55108, USA

[5] Biochemistry, Molecular Biology & Biophysics Graduate Program, University of Minnesota – Twin Cities, Minneapolis, MN 55455 USA

[6] Characterization Facility, College of Sciences and Engineering, University of Minnesota – Twin Cities, Minneapolis, MN 55455 USA

* Corresponding authors: mansky@umn.edu; zhangwei@umn.edu

Keywords: retrovirus; lentivirus; virus-like particle; maturation; morphology

Running title: HIV-2 capsid protein mutagenesis

Word count: 3780

Abstract

Human immunodeficiency virus (HIV) Gag drives virus particle assembly. The capsid (CA) domain is critical for Gag multimerization, and encodes key residues that dictate Gag-Gag interactions and particle morphology. Previous studies have demonstrated that the immature particle morphology of HIV-2 is intriguingly different relative to that of HIV-1. Based upon this observation, we sought to define the critical determinants for Gag-Gag interactions and investigate the comparative differences between HIV-1 and HIV-2 by conducting site-directed mutagenesis of targeted locations in HIV-2 CA. In particular, a panel of 31 site-directed mutants of residues that reside at the HIV-2 CA inter-hexamer interface, intra-hexamer interface and CA inter-domain linker were created and analyzed for their impact on the efficiency of particle production, particle morphology, particle infectivity, Gag subcellular distribution and *in vitro* protein assembly. Seven conserved residues (L19, A41, I152, K153, K157, N194, D196) and two non-conserved residues (G38, N127) were found to significantly impact Gag multimerization and particle assembly. Taken together, these observations complement structural analyses of immature HIV-2 particle morphology and Gag lattice organization as well as provide important comparative insights into the determinants responsible for the observed morphological differences between HIV immature particle morphology and its association with virus replication and particle infectivity.

Word count = 202

45 ## Importance

46 The retroviral Gag polyprotein is known to drive particle assembly, and the capsid (CA) domain is a
47 critical determinant for Gag multimerization and immature particle morphology. Intriguingly, the immature
48 particle morphology of human immunodeficiency virus type 2 (HIV-2) is distinctly different relative to that
49 of HIV type 1 (HIV-1). In order to aid in the identification of the critical determinants responsible for the
50 observed morphological differences, we conducted site-directed mutagenesis in targeted locations of the
51 HIV-2 CA. Our results have identified conserved and non-conserved amino acid residues that impact
52 Gag multimerization, particle assembly, virus replication, and infectivity.

53

54 **Word count** = 97

55 ## Introduction

56 Human immunodeficiency virus (HIV) belongs to the lentivirus genus of the *Retroviridae*. To date,
57 HIV has infected more than 70 million people worldwide (1). HIV comprises two main types, HIV type 1
58 (HIV-1) and HIV type 2 (HIV-2), which clearly have similar modes of replication, transmission, and clinical
59 symptomatology (2). Despite these similarities, there are notable differences in the general prevalence,
60 rate of transmission, and relative particle infectivity between these viruses. For example, relative to HIV-1,
61 HIV-2 has attenuated prevalence and is mainly found in West Central Africa, with reduced infectivity and
62 transmissibility (2, 3). HIV-2 is known to have lower viral loads during the course of the infection, slower
63 rates of $CD4^+$ T-cell decline, and delayed clinical progression to AIDS (4). Individuals infected with HIV-2
64 are typically less infectious in the early stages of infection and can more readily lead to long-term
65 nonprogressors (5, 6). Different steps in the HIV life cycle have been successfully targeted by combined
66 antiretroviral therapy (ART), leading to a remarkable reduction in overall morbidity and mortality (7).

67 The HIV assembly pathway represents a promising and generally underdeveloped target for
68 antiretroviral intervention. While intensive efforts have been made to date to target HIV assembly (8-12),
69 approved antiretroviral drugs to date have been elusive. The HIV capsid (CA) has been viewed as a
70 particularly promising antiviral drug target due to the fact that its stability and integrity are critical for virus
71 replication and particle infectivity (13). For example, lenacapavir (LEN, GS-6207, GS-CA2), an
72 investigational first-in-class long-acting HIV-1 CA inhibitor, is currently in phase 2/3 clinical trials and is
73 seeking regulatory approval (14). LEN binds to the hydrophobic pocket formed by two adjoining CA
74 subunits within the CA hexamer. Since HIV-2 is not susceptible to many anti-HIV-1 drugs (15, 16),
75 insights into the molecular basis for antiretroviral drug susceptibility can inform the development of
76 effective, next-generation treatments for both HIV types.

77 The HIV Gag polyprotein is the major structural protein responsible for driving retrovirus assembly
78 (12). Comparatively, the HIV-1 (NL4-3) and HIV-2 (ROD) Gag proteins have a moderate level of amino
79 acid sequence conservation (i.e., 59% identity, 72% similarity). HIV assembly engages three key Gag
80 domains: the matrix (MA) domain is responsible for Gag-membrane binding (17, 18); the nucleocapsid
81 (NC) domain interacts with the viral RNA packaging signal and encapsidates the viral genome (19); and

82 the CA domain is critical for Gag multimerization during virus assembly and core formation during virus
83 maturation. The CA domain has two structurally distinct subdomains, i.e., the CA amino-terminal
84 subdomain (CA_{NTD}) and the CA carboxy-terminal subdomain (CA_{CTD}) (20), which are connected by a
85 flexible inter-domain linker. The major homology region (MHR), a 20-residue segment (amino acid
86 residues 153-172 in HIV-1 CA) toward the amino-terminus of the CA_{CTD}, is highly conserved. During
87 particle assembly, Gag ($Pr55^{Gag}$) oligomerizes at the plasma membrane, forming a radially arranged
88 lattice that curves and deforms the plasma membrane (17). Formation of the immature Gag lattice drives
89 budding and release of immature particles. The virally-encoded protease (PR) processes the Gag
90 polyprotein to create mature MA, CA and NC proteins that are needed to form a mature virion (21). The
91 MA protein remains associated with the inner leaflet of the viral membrane, the CA protein reassembles
92 into a cone-shaped core that contains a dimeric viral genomic RNA coated with NC protein (17).
93 The morphologies of HIV-1 immature and mature particles have been intensively studied (22, 23).
94 Previous observations indicate that the overall mature HIV-1 particle is made from a lattice of ~250 CA
95 hexamers closed by the insertion of 12 CA pentamers (24). However, there are no pentamers in the
96 immature HIV-1 Gag lattice since the pentamers mediate areas of high curvature of the mature conical
97 core that are not present in the immature lattice. The CA hexamer contains an inner ring of six CA_{NTD}
98 subdomains held together by contacts between adjacent CA molecules (25, 26). The interactions
99 between CA monomers are related by six-fold symmetry within a hexamer (i.e., intra-hexamer) and by
100 three-fold and two-fold symmetry between neighboring hexamers (i.e., inter-hexamer). The hexamers are
101 stabilized by interactions at these interfaces (24).
102 To date, intriguing and surprising differences have been discovered between the immature Gag lattice
103 structure of HIV-1 and other retroviruses, although the HIV-1 and HIV-2 CA domains have a moderate
104 level of amino acid sequence conservation. Moreover, many immature Gag lattice structures have been
105 published, including Rous sarcoma virus (RSV) (27), Murine leukemia virus (MLV) (28), and HIV-1 (29).
106 It is well recognized that key amino acid residues in CA can dictate virus particle morphology.
107 Mutagenesis studies have been used to confirm the importance of the interface residues for core
108 morphology and stability and virion infectivity (24, 25, 30, 31). Mutations in the CA domain of Gag have

109 been shown to affect particle assembly and virion infectivity in different retroviruses, including HIV-1 (32),
110 Simian immunodeficiency virus (SIV) (33), Mason-Pfizer monkey virus (M-PMV) (34), and RSV (35).
111 Several key mutants, for example the HIV-1 CA W184A and M185A cause Gag assembly defects,
112 produce non-infectious virus particles, reduce CA dimerization and intermolecular Gag–Gag interactions
113 *in vitro*, diminish immature particle production *in vivo*, and abolish CA dimerization (30, 36); similar
114 studies have been done with SIV (33). In addition to site-directed mutagenesis, residue swaps between
115 closely related viruses have been used to assess mutant effects on particle production and infectivity.
116 For example, a previous study of HIV-1 and SIVmac residues swaps in HIV-1 CA Helix 7, such as E128N,
117 I141C, were found to cause severe reductions in particle production and infectivity when swapped to the
118 corresponding SIVmac residue (37). This indicated that some non-conserved amino acids in HIV-1 CA
119 Helix 7 have important roles in assembly and particle infectivity.
120 Given these observations, we hypothesized that differences between HIV-1 and HIV-2 Gag CA
121 interactions could help explain the distinct morphological differences observed, and provide insights into
122 the role of particle morphology on particle infectivity. To investigate this, a panel of site-directed mutants
123 were analyzed for their impact on the efficiency of immature particle production. Selected mutants were
124 additionally analyzed for mature particle production, infectivity, Gag subcellular distribution and *in vitro*
125 protein assembly. This integrative analyses discovered critical residues and novel CA-CA interactions
126 involved in HIV-2 CA that are crucial for virus particle assembly and infectivity. Taken together, our
127 studies provide mechanistic detail regarding the CA residues that mediate viral particle assembly,
128 highlight fundamental differences between HIV-1 and HIV-2 CA, and provide further insight into the
129 fundamental aspects of HIV particle assembly that can inform antiretroviral intervention therapies.
130

131 ## Results

132 **Identification of conserved HIV-2 CA residues that impact immature particle production.** Previous
133 observations have indicated that specific amino acid residues in the Gag CA domain encode the key
134 determinants that dictate CA-CA interactions and immature and mature virus particle morphology for a
135 number of retroviruses, including HIV-1, MLV, and RSV (27-29, 38, 39). To date, limited data regarding
136 HIV-2 Gag CA residues that impact particle assembly have been described. To identify critical residues
137 in HIV-2 Gag CA that mediate HIV particle assembly, we used previous studies in HIV-1 and HIV-2 to
138 guide our studies (30, 36, 40) (**Fig. 1**). Next, we conducted alanine-scanning mutagenesis in targeted
139 locations of the CA protein that were implicated in encoding critical amino acid residues important for CA-
140 CA interactions that impact virus particle assembly. A panel of twenty-one mutants were created and
141 analyzed for their influence on the efficiency of particle production by using immunoblot analysis with a
142 tractable HIV-2-like particle system that mimics authentic, immature virus particle assembly and release
143 (**Fig. 2**). In particular, we conducted ten site-directed mutants at the HIV-2 CA_{NTD}-CA_{CTD} linker domain
144 (**Fig. 2A**). Two mutations I152A and K153A were discovered to reduce immature particle production
145 relative to WT by 3.9-fold, and 4-fold, respectively (**Fig. 2A**). These residues are located in the MHR
146 region. Notably, some conserved residues in HIV-1 MHR (e.g., HIV-1 Q155N) led to a dramatic reduction
147 in HIV-1 immature particle production (41). Notably, the I152A mutant of HIV-2 CA has not been
148 analyzed with the appropriate corresponding mutant in HIV-1 CA (i.e., I153A).

149 Five site-directed mutants of residues at the intra-hexamer interface were analyzed, with four of them
150 (i.e., L19A, K157A, N194A, and D196A) resulting in a 2-fold or greater reduction in immature particle
151 production relative to that of WT (**Fig. 2B**). The HIV-2 CA L19A and N194A mutants reduced particle
152 production by 4.5-fold and 3.5-fold, respectively, compared to WT. The comparable residues have not
153 been characterized to date in the HIV-1 CA domain. The HIV-2 CA K157A and D196A mutants resulted
154 in 2.1-fold and 2.8-fold reductions in particle production, respectively, compared to WT. This observation
155 is similar to that reported with comparable mutations in the HIV-1 CA domain on particle production (30,
156 36, 42). Four site-directed mutants at the two-fold inter-hexamer interface and two mutants at the three-
157 fold inter-hexamer interface were analyzed for their influence on particle production (**Fig. 2C**). The two-

158 fold inter-hexamer interface mutants had particle production efficiencies comparable to that of WT except
159 for the N20A mutant, which had a minor reduction in particle production (~92% of WT). One of the two
160 mutants at the three-fold inter-hexamer interface, i.e., A41D, had a 4.6-fold reduction in particle
161 production (**Fig. 2C**).

162 **Identification of non-conserved HIV-2 CA residues and their impact on immature particle**
163 **production.** Previous studies have demonstrated striking morphological differences between HIV-1 and
164 HIV-2 immature particles, which helps support a model in which relatively minor changes in protein-
165 protein interaction geometry can profoundly impact overall particle morphology (39). To further
166 investigate HIV-2 CA-CA interactions, a panel of 10 site-directed mutations at non-conserved CA
167 residues were analyzed by mutating each HIV-2 CA residue to the corresponding HIV-1 amino acid
168 residue (**Fig. 3A**). Two HIV-2 CA mutants (i.e., G38M and N127E) reduced particle production by greater
169 than 50% compared to that of WT. These amino acid residues are both located at the three-fold inter-
170 hexamer interface in the CA_{NTD}, based upon structural comparison to the HIV-1 lattice structure. The
171 HIV-2 G38M mutation reduced both immature particle production (**Fig. 3A**) and mature particle
172 production (**Fig. 3C**). HIV-1 M39G mutation was found to also reduce particle production relative to that
173 WT (**Fig. 3E**).

174 It was previously observed that mutation of the HIV-1 CA E128 residue to the corresponding HIV-2
175 residue (i.e., HIV-1 E128N) reduced viral replication (37). We observed the HIV-2 N127E mutant reduced
176 immature particle production by 4.3-fold compared to that of WT (**Fig. 3A**), and resulted in a 6.7-fold
177 reduction of mature particle production compared to WT (**Fig. 3C**). The HIV-1 E128N mutant led to a 2.6-
178 fold reduction of mature particle production compared to WT. Analysis of the position of E128 in the HIV-
179 1 immature CA cryo-EM structure (22) reveals that E128 is within interaction distance (<4 Å) with the
180 E45 residue. Based upon the HIV-2 sequence, two single mutations (i.e., HIV-2 E44N, N127E) were
181 generated to compare to that of WT (E44/N127). Production of immature particles for the E44N and
182 N127E mutants were about 4-fold less than the WT (**Fig. 3B**). To assess if these residue positions in
183 HIV-2 may interact with one another, we created the HIV-2 E44N/N127E double mutant, which led to a
184 doubling of immature particle production compared to the single mutants, but was 2-fold less than WT.

185 **Perturbation of Gag subcellular distribution.** Gag subcellular distribution can alter Gag
186 multimerization and productive particle assembly and release (17). To determine if the subcellular
187 distribution of HIV-2 Gag mutants was associated with reductions in immature particle production,
188 selected mutants were engineered to contain a YFP tag at the carboxy-terminus of the Gag protein. The
189 mutants analyzed included L19A (intra-hexamer interface), A42D (inter-hexamer interface), I152A
190 (located at the CA_{NTD}-CA_{CTD} linker domain), and the non-conserved G38M and N127E mutants. HIV-2
191 WT and mutant Gag-YFP constructs were transfected into Hela cells, and analyzed for their ability to
192 multimerize and form Gag puncta, particularly at the plasma membrane (39). Among the five mutants
193 analyzed, the HIV-2 G38M and N127E mutants revealed a diffuse fluorescence in the cytoplasm along
194 with enrichment within or immediately surrounding the nucleus (**Fig. 4**). These observations indicated
195 that the G38M and N127E mutations (which are non-conserved residues in the three-fold interface)
196 perturb Gag subcellular localization.

197 **G38M and N127E alter HIV-2 immature particle morphology.** Information regarding the critical
198 residues of HIV-2 CA that dictate particle morphology is limited in comparison to that of HIV-1 CA.
199 Previous reports have identified surprising and intriguing differences between the immature Gag lattice
200 structure of HIV-1 and other retroviruses (27-29, 38). The striking morphological differences between
201 immature WT HIV-1 and HIV-2 particles was notable and implies that relatively minor changes in the
202 geometry of protein-protein interactions can significantly impact overall particle morphology (39).
203 The HIV-2 CA G38M and N127E mutants were next examined for their influence on immature
204 particle morphology, and to contrast them to HIV-2 WT immature particles, which have a uniform particle
205 morphology (39) (**Fig. 5A**). In particular, HIV-2 WT immature particles have a tightly packed Gag lattice,
206 implying a highly organized CA layer below the viral membrane. The majority of the HIV-2 WT immature
207 particles were spherical, with a small population having other morphologies (**Fig. 5A**). In contrast, about
208 25% of HIV-2 G38M (**Fig. 5B**) and N127E (**Fig. 5C**) immature particles were observed to have non-
209 spherical morphologies. Also, most G38M and N127E mutant immature particles did not have an
210 organized CA lattice below the lipid bilayer, suggesting that the G38M and N127E mutations impose a
211 defect in Gag multimerization to form a proper Gag lattice structure.

212 **The G38M and N127E mutations severely diminish HIV-2 particle infectivity.** Infectivity assays of CA
213 point mutants help determine whether a single amino acid can alter virus replication. Here, a single-cycle
214 infectivity system with a fluorescent reporter system was used as previously described (43). Vector virus
215 particles (WT or mutant) were harvested from producer cells and used to infect permissive target cells
216 and assessed by flow cytometry. Relative infectivity of mutants compared to WT was determined.
217 The HIV-2 G38M and N127E mutants exhibited severe defects in particle infectivity, 100-fold and 56-
218 fold reductions compared to WT, respectively (**Fig. 3D**). To assess if the equivalent mutations in HIV-1
219 (see **Fig. 1A**) impact particle infectivity, the site-directed mutant HIV-1 CA M39G was analyzed and was
220 found to have a 100-fold reduction in particle infectivity compared to WT (**Fig. 3F**). A previous analysis of
221 the HIV-1 CA N128E found that this mutant reduced infectivity 50-fold compared to WT (37).

222 **Mutations disrupt in vitro HIV-2 CA-NC assembly.** The use of *in vitro* protein assembly assays have
223 been very useful for analyzing Gag-Gag interactions due to this being an efficient system to perturb CA-
224 CA interactions in the absence of other cellular effects (44). To assess the impact of selected HIV-2 CA
225 mutations on CA-CA interactions, a HIV-2 CA-NC protein expression construct was used to make
226 purified recombinant protein from *E. coli* for *in vitro* assembly assays. Purified protein was dialyzed
227 against assembly buffer conditions to induce helical assemblies to form (for WT HIV-2 CA-NC protein),
228 and quantified by reaction turbidity at A340 nm based on an established model where turbidity reflects
229 the state of protein assembly (45, 46). Based upon the severe reduction of immature particles (**Fig. 3,**
230 **4A**), L19A, A42D, I152A, G38M and N127E were analyzed every 20 min for 2h (**Fig. 6**).
231 The normalized A340 nm reading for HIV-2 WT peaked at 20 min (i.e., 1.27), then slowly decreased
232 and remained stable (i.e., 0.56) (**Fig. 6A**). HIV-2 L19A, G38M, and I152A had similar trends with WT, but
233 with normalized A340 nm values 1.77, 0.34, and 0.65, respectively (**Fig. 6**). N127E reached a peak at 40
234 min, with an A340 nm value of 0.36, while A41D had low turbidity readings (i.e., < 0.36) during the
235 experimental time course (**Fig. 6**). G38M, A41D, N127E and I152A had decreased assembly kinetics
236 relative to that of WT.
237 At the final endpoint (120 minutes), G38M, A41D, N127E, and I152A had significant reductions in
238 turbidity relative to WT, which were 7.0-fold (i.e., G38M, N127E, I152A) or 25-fold (A41D) lower than that

239 of WT (**Fig. 6G**). These observations support the conclusion that these mutants form unstable assembly
240 products that disrupt CA-NC helical assembly, except for L19A. These observations indicate these
241 residues play critical roles in the formation of CA-NC helical assemblies. Previous studies of HIV-1 A42D
242 CA-NC protein assembly were also shown to impair helical assembly formation (44), which is in good
243 agreement with our observations with HIV-2 A42D.

244 Visualization of these CA-NC helical assemblies by negative stain TEM reveals that HIV-2 WT CA-
245 NC assembled into stable, regularly ordered uniform tubular structures, while G38M, A41D, N127E, and
246 I152A did not (**Fig. 6H**). The L19A CA-NC mutant resulted in protein aggregations without uniform
247 tubular structures, suggesting that the observed turbidity was due to large protein aggregates versus
248 ordered helical tubes. Taken together, these results provide evidence for HIV-2 CA mutants had defects
249 in CA-CA interactions that prevented helical tube formation.

250 ## Discussion

251 Particle morphologies among retroviral genera are quite distinct, indicating a diversity of
252 morphologies that are different from that of HIV-1(39). Intriguingly, HIV-2 also produces immature
253 particles that are morphologically distinct from that of HIV-1 – *i.e.,* they possess a nearly complete
254 immature Gag lattice, have a larger than average particle diameter, and have a relatively higher average
255 copy number of incorporated Gag (39). However, to our knowledge, this is the first time a panel of HIV-2
256 mutants have been used to analyze HIV-2 Gag-Gag interactions.

257 The primary goals of our experiments were two-fold: first, to investigate the critical role of the HIV-2
258 CA in Gag-Gag interactions and virus particle assembly; and second, to identify differences between
259 HIV-1 and HIV-2 CA domains that alter particle assembly. We created a panel of 31 site-directed
260 mutants to achieve these goals (**Fig. 1**). This panel of 31 mutants encompassed 21 alanine-scanning
261 mutants at highly conserved residues in HIV-2 CA, and 10 site-directed mutants at non-conserved
262 residues (*i.e.,* swapping the native HIV-2 residue to the corresponding residue observed in HIV-1 CA).

263 This approach allowed for an interrogation of key selected residues in the HIV-2 CA domain of Gag,
264 based upon their predicted location at the CA intra-hexamer interface, the inter-hexamer interface, and
265 the linker domain. To aid in our selection of mutants, specific residues were chosen based upon a
266 structural comparison between HIV-1 and HIV-2 CA, as well as previous on HIV-1 CA structure (30, 36,
267 37, 44, 47). Mutants that resulted in a disruption of productive Gag-Gag interactions (*i.e.,* a two-fold or
268 greater decrease in particle production) were selected for subsequent analyses. The majority of the
269 mutants analyzed had no overall effect on immature particle production. In particular, seven of the
270 mutants at conserved amino acid residues (*i.e.,* L19A, A41D, I152A, K153A, K157A, N194A, D196A)
271 (**Fig. 2**) and two mutants at non-conserved residues (*i.e.,* G38M, N127E) (**Fig. 3A**) had a significant
272 impact on Gag-Gag interactions and efficient particle assembly.

273 For mutants at conserved residues and for the mutants at the HIV-2 CA_{NTD}-CA_{CTD} linker domain,
274 there was no significant reduction in immature particle production unless they were at the MHR domain
275 (**Fig. 2A**). Mutants at the intra-hexamer interface were observed to reduce particle production (**Fig. 2B**).
276 Furthermore, mutants at the three-fold interface, but not at the two-fold interface, significantly reduced

277 particle production (**Fig. 2C**), indicating that the residues at the intra-hexamer interface and at the three-
278 fold inter-hexamer interface are critical for immature particle production and CA-CA interactions.
279 Importantly, several key residues, including L19, I152 and N194, had not been previously reported for
280 either HIV-2 or HIV-1.

281 A particularly notable discovery was two key mutants (G38M and N127E) at non-conserved residues.
282 Intriguingly, the key features of the HIV-2 CA G38M and N127E Gag variants included a significant
283 reduction of immature and mature particle production (**Fig. 3A, C**). This observation indicates that these
284 mutations impact one or more steps in the particle assembly pathway. Furthermore, these mutants
285 demonstrate a complete loss of particle infectivity (**Fig. 3D**). Gag subcellular distribution revealed an
286 increase in nuclear and perinuclear localization for the G38M and N127E mutants relative to that of WT
287 (**Fig. 4**). Direct visualization of immature particles by using cryo-EM revealed an absence of electron
288 density below the viral membrane (**Fig. 5**). The ability of CA to form oligomers in a cell-free assay
289 demonstrated that these two CA variants significantly disrupt HIV-2 CA-NC protein assembly, given that
290 no ordered assemblies were observed (**Fig. 6**). To assess the structural basis of these results, we
291 analyzed the molecular interfaces in HIV-1 lattice structures from both immature and mature virus
292 particles. The HIV-1 E128 residue on helix 7 is within interaction distance (< 4Å) to E45 on helix 2 in the
293 immature CA lattice three-fold interface. Using this structural comparison, we chose to further probe the
294 homologous HIV-2 residue E44 and its potential interaction partner (*i.e.,* N127). Two mutations in HIV-2,
295 E44N and N127E, resulted in significant particle reduction individually, but the double mutant (*i.e.,*
296 E44N/N127E) had a partial rescue in particle production, suggesting that these residues are involved in a
297 direct interaction in the immature HIV-2 Gag lattice (**Fig. 3B**). This provides evidence for an
298 undiscovered HIV Gag-Gag interaction in HIV-2 between residues E44 and N127.

299 Our results demonstrate that relatively minor changes in CA residues could profoundly impact overall
300 particle assembly. Non-conserved residues such as G38 and N127 likely play a critically important role in
301 HIV-2 CA structure and Gag-Gag interactions. Intriguingly, the G38 and N127 residues are critical
302 residues in the HIV-2 CA three-fold inter-hexamer interface, implying that the three-fold interface likely
303 plays a critical role in Gag-Gag interactions.

304 One potential limitation of our study is that not all residues in the HIV-2 CA domain of Gag were
305 analyzed. Residues were identified for site-directed mutagenesis based on a variety of parameters
306 including mutants (i) at the CA: inter-domain linker, intra-hexamer interface, and inter-hexamer interface
307 (two-fold interface & three-fold interface); (ii) at conserved and non-conserved residues; (iii) at residues
308 in helices and loops; (iv) and previously reported and not reported. While not exhaustive, the panel of
309 mutants have revealed novel residues not previously described as important for HIV particle assembly.
310 Future studies may likely identify other important residues. Finally, analysis of novel mutants and their
311 impact on viral infectivity through the identification of second-site reversion mutations would further aid in
312 gaining a deeper understanding of CA-CA and Gag-Gag interactions important for virus particle
313 assemble and infectivity.
314 The observations in this current study provide an important complement to structural analyses of
315 HIV-2 immature and mature particle morphologies, and help provide important insights into the structure-
316 function relationship between HIV particle morphology and virion infectivity. Furthermore, these studies
317 highlight the importance of comparative virology in providing important insight into differences that can
318 advance knowledge in our fundamental understanding of HIV assembly and replication.

319 # MATERIALS AND METHODS

320 **Plasmids, cell lines, and reagents. The** HIV-2 Gag expression plasmids, pN3-Gag and pEYFP-N3-Gag,
321 as well as the HIV-2 Env expression plasmid have been previously described (39). HeLa and
322 HEK293T/17 cells lines were purchased from ATCC (Manassas, VA) and cultured in Dulbecco's modified
323 Eagle medium (DMEM) supplemented with 10% fetal clone III (FC3; GE Healthcare Lifesciences, UT)
324 and 1% Penicillin-Streptomycin (Pen Strep; Invitrogen, CA) at 37 °C in 5% CO_2. The HIV-1 and HIV-2
325 single-cycle vectors, *i.e.,* pNL4-3 MIG (48) and pROD-MIG (49) have been previously described,
326 respectively. Vector viruses were pseudotyped with the VSV-G expression construct, pHCMV-G (J.
327 Burns, UCSD, San Diego, CA). U373-MAGI-CXCR4$_{CEM}$ cells (NIH AIDS Reagent Program, NIAID, NIH)
328 were maintained similarly to HEK293T/17 cells, supplemented with 1.0 µg/mL puromycin, 0.1 mg/mL
329 hygromycin B, and 0.2 mg/mL neomycin to the medium. All cells used in this study were certified as
330 being mycoplasma-free.

331 **Site-directed mutagenesis of Gag expression plasmids.** A panel of 31 alanine-scanning mutants (**Fig.**
332 **1A**) were created in the HIV-2 CA domain of Gag. Among this panel, 21 alanine-scanning HIV-2 CA
333 mutants at conserved residues were in the pN3-Gag plasmid of HIV-2 Gag (except A41D) by using the
334 Gibson assembly method as previously described (50). A panel of 10 non-conserved HIV-2 CA mutants
335 were generated by changing the codons in HIV-2 to HIV-1 NL4-3 residues in the HIV-2 Gag pN3-Gag
336 expression plasmid. Selected mutants of interest were also introduced into the pEYFP-N3-Gag, pROD-
337 MIG, and pET28a plasmids for cellular localization, infectivity, and in vitro assembly studies, respectively.
338 All mutants were confirmed by Sanger sequencing.

339 **Virus particle production.** The efficiency of immature particle production was analyzed by quantifying
340 Gag proteins in released particles by harvesting cell culture supernatants by using immunoblot analysis
341 with a mouse monoclonal anti-HIV-1 p24 antibody (Catalogue #: sc-69728; Santa Cruz Biotechnology,
342 TX). Briefly, the pN3-HIV-2-Gag plasmid and the HIV-2 Env expression plasmid were co-transfected into
343 HEK293T/17 cells by using GenJet, ver II (SignaGen, Gaithersburg, MD) at a 10:1 ratio, respectively.
344 After 48-h post-transfection, the viral supernatants were harvested, clarified by centrifugation (1,800 × g

345 for 10 min), and filtered through 0.2 μm filters. Next, the filtered cell culture supernatants were
346 concentrated by ultracentrifugation in a 50.2 Ti rotor (Beckman Coulter, CA) at 211,400 × g for 90 min
347 through an 8% Opti-prep (Sigma-Aldrich, MO) cushion. Particle pellets were resuspended in 1× STE
348 buffer (100 mM NaCl, 10 mM Tris pH 8.0, and 1 mM EDTA) (G-Biosciences, MO). The 293T/17 cells
349 were collected and lysed with RIPA lysis buffer and clarified via centrifugation (1800 x g for 10 min). The
350 protein concentrations were measured by using the BCA assay (Pierce, Rockford, IL) before the samples
351 were subjected to SDS-PAGE and then transferred to nitrocellulose membranes. The Gag proteins were
352 detected with a 1:1,500 dilution of anti-HIV p24 antibody in 5% milk TBST (Tris-buffered saline plus
353 Tween-20). Glyceraldehyde 3-phosphate dehydrogenase (GAPDH) was detected by using a 1:1,000
354 anti-GAPDH hFAB™ Rhodamine antibody (Bio-Rad, Hercules, CA) in 5% milk TBST (Tris buffer saline
355 plus Tween-20). Membranes were washed before incubation with a goat anti-mouse StarBright™ Blue
356 700 secondary. Gag expression levels in cells were normalized relative to GAPDH levels, and the mutant
357 Gag expression levels were determined relative to that of WT HIV-2 Gag.
358 The efficiency of mature particle production was analyzed by quantifying Gag by detection of the CA
359 (p24) band from cell culture supernatants. Briefly, the HIV-2 pROD-MIG and the VSV-G expression
360 plasmids were co-transfected into HEK293T/17 cells by using GenJet ver II at a 3:1 molar ratio to
361 produce both WT and mutant virus particles. Forty-eight hours post-transfection, the cell culture
362 supernatants were harvested, clarified by centrifugation (1,800 × g for 10 min), and filtered through 0.2
363 μm filters. The supernatants were then concentrated by ultracentrifugation in a 50.2 Ti rotor (Beckman
364 Coulter, CA) at 211,400 × g for 90 min through an 8% Opti-prep (Sigma-Aldrich, St. Louis, MO) cushion.
365 Capsid proteins were detected with a 1:1,500 anti-HIV p24 antibody. Glyceraldehyde 3-phosphate
366 dehydrogenase (GAPDH) was detected with 1:1,000 anti-GAPDH hFAB™ Rhodamine antibody (Bio-
367 Rad). The CA levels from cells were normalized relative to GAPDH levels, and the CA mutant expression
368 levels were determined relative to that of WT HIV-2 Gag. Membranes were washed before incubation
369 with 1:2,500 goat anti-mouse StarBright™ Blue 700 (Bio-Rad).
370 The membranes from immunoblot analyses were imaged by using a ChemiDoc Touch system (Bio-
371 Rad, CA) and analyzed with ImageJ. Results were analyzed by using GraphPad Prism 6.0 (GraphPad

372 Software, Inc., CA). Relative significance between a mutant and WT was determined by using an
373 unpaired t-test. Immunoblot analyses were done by conducting three independent replicates.

374 **Gag subcellular distribution analysis.** Gag subcellular distribution was analyzed by quantifying the
375 degree of Gag puncta formation in cells by using confocal laser scanning microscopy to localize Gag-
376 eYFP as previously described (51). Briefly, HeLa cells were cultured in six-well plates on 1.5 standard
377 glass coverslips coated with Poly-L-lysine as previously described (51). HeLa cells were transiently
378 transfected with EYFP-tagged Gag; untagged Gag expression plasmids at a 1:4 molar ratio by using
379 GenJet, ver II (SignaGen, Gaithersburg, MD). At 48-h post-transfection, cells were stained by using DAPI
380 (Thermo Fisher Scientific, MA) and ActinRed 555 (Invitrogen, CA) prior to before fixation with 4%
381 paraformaldehyde (Thermo Fisher Scientific, MA). Cells were imaged by using a Zeiss LSM 700 confocal
382 laser scanning microscope with a Plan-Apochromat 63×/1.40-numeric-aperture (NA) oil objective at 1.2×
383 zoom (Carl Zeiss, Oberkochen, Germany). At least 5 individual cells were imaged from three
384 independent experimental replicates, for a total of 15 cells for each Gag mutant and WT Gag.

385 **Cryo-EM analysis of particle morphology.** The pN3-HIV-2-Gag plasmid and the HIV-2 Env expression
386 plasmids were co-transfected into HEK293T/17 cells by using GenJet, ver II at a 10:1 molar ratio as
387 previously described (39). At 48-h post-transfection, cell culture supernatants were harvested and
388 centrifuged at 1,800 × g for 5 min and followed by passing through a 0.2 µm filter. Particles were then
389 concentrated by ultracentrifugation in a 50.2 Ti rotor at 211,400 × g for 90 min through an 8% Opti-prep
390 cushion. Particle pellets were resuspended in about 200 µl of STE buffer prior to ultracentrifugation
391 through a 10% to 30% Opti-Prep step gradient at 301,090 x g for 3 h. The particle band was removed
392 from the gradient by puncturing the side of the centrifuge tube with a hypodermic syringe needle and
393 pelleted in STE buffer at 267,636 × g for 1 h by using an SW55 Ti rotor. The resulting particle pellet was
394 then resuspended in approximately 10 µl STE buffer and frozen at -80°C until analyzed by cyro-EM.
395 Experiments were done in triplicate. Samples were initially screened by negative staining TEM with 0.75 %
396 (w/v) uranyl formate by using a 120 kV Tecnai Spirit TEM (52).

397 Cryo-EM analysis of particles were done as previously described (39, 51, 53). Briefly, particle
398 samples were thawed on ice, and approximately 3.5 µL of purified virus particles were applied to freshly

399 glow-discharged (10 mA for 30 sec using a Leica Ace600 glow-discharger) Quantifoil R2/1 300-mesh
400 holey carbon-coated copper grids. The grids were then blotted for 4-10 sec with filter paper at 19°C with
401 85% relative humidity and plunge-frozen in liquid ethane using a FEI Mark III Vitrobot or Leica GP-2 grid
402 plunger. The frozen grids were stored in liquid nitrogen until imaging analysis.
403 Cryo-EM analysis was done by using a Tecnai FEI G2 F30 FEG transmission electron microscope
404 (FEI, Hillsboro, OR) at liquid nitrogen temperature operating at 300 kV. Images were recorded at a
405 nominal magnification of 39,000x and 59,000x magnification under ~25 electrons/$Å^2$ conditions at 1 to 5
406 µm under-focus by using a Gatan Slow Scan 4k by 4k charge-coupled-device (CCD) camera or a Gatan
407 K2 Summit direct electron detector (Gatan Inc., Pleasanton, CA).

408 **Virus infectivity assay.** The HIV-2 pROD-MIG and VSV-G expression plasmids were co-transfected
409 into HEK293T/17 cells by using GenJet, ver II at a 3:1 molar ratio to produce WT and mutant particles.
410 Forty-eight hours post-transfection, cell culture supernatants were harvested, clarified by centrifugation
411 (1,800 × g for 10 min), and filtered through a 0.2 µm filter. U373-MAGI-CXCR4 cells were plated in a 12-
412 well plate and 1 ml of concentrated cell culture supernatant along with 1 ml fresh medium were added
413 per well. Each mutant was analyzed in a quadruplicate. The cells were collected to detect virus-infected
414 cells via flow cytometry by using a BD LSR II flow cytometer (BD Biosciences, San Jose, CA)) at 48-h
415 post-infection (43). Data were analyzed by using FlowJo v.7 (FloJo Inc, Ashland, OR). Infected cells
416 were determined by identification of all quadrants expressing either or both fluorescence markers (i.e.,
417 mCherry, GFP, and both mCherry/GFP) relative to that of WT vector virus. Relative infectivity was
418 normalized to particle production as determined by immunoblot analysis of cell culture supernatants.
419 Experiments were conducted in triplicate

420 **Cell-free HIV-2 CA-NC assembly analysis. The** HIV-2 CA-NC (Gag amino acids 136-431) was cloned
421 into the pET28a bacterial expression plasmid, with mutants created by using the Gibson assembly
422 procedure. Protein is expressed in *E. coli* by using as previously described (45, 46). Briefly, the CA-NC
423 protein was expressed in BL21 (DE3) RIP pLysS *E. coli* grown in 200 mL of ZY-auto induction media in a
424 platform shakers for 16 h at 37C (54). Cells were pelleted and resuspended in 50 mL lysis buffer per 200
425 mL culture (500 mM NaCl, 25 mM Tris pH 7.5, 1 µM $ZnCl_2$, 10 mM β-Mercaptoethanol (BME)) and then

426 exposed to flash freezing to aid in cell lysis. After thawing, cells were lysed by adding 10 mg lysozyme,
427 0.1% Triton (v/v), and sonicated for 10 sec on/off cycles at 40% amplitude for three, 5 min treatments to
428 reduce viscosity. The cell lysate was clarified by centrifugation 12,000 × g 40 min. Nucleic acids were
429 removed by using 0.11 (v/v) 2M ammonium sulfate and 0.11 (v/v) polyethyleneimine (PEI), and protein
430 subsequently precipitated by using saturated ammonium sulfate with 1/3 (v/v) of the total supernatant
431 volume. The precipitated protein was pelleted by centrifugation at 7,500 × g spin for 15 min. The
432 precipitate was then resuspended in 50 mM NaCl, 25 mM Tris, 5 μM $ZnCl_2$, 10 mM BME, pH 7.5, and
433 further dialyzed against 1L for 1 h at 4C. The protein was concentrated using an Amicon ultra-15
434 centrifugal filter unit concentrator (Millipore, Burlington, MA) and loaded onto an ion-exchange column
435 (HiTrap SP FF, Cytiva, Global Life Sciences Solutions USA LLC, Marlborough, MA). Protein was eluted
436 by using a linear NaCl gradient from 50-700 mM. Fractions containing the protein were pooled,
437 concentrated to ~10 mg/mL, and flash-frozen in liquid nitrogen. Only samples below a 0.6 A260/A280
438 ratio were used for further analysis to ensure no significant nucleic acid contamination was affecting the
439 assembly kinetics or products.
440 The CA-NC assembly reactions were done using purified protein diluted to 50 μM in 250 mM NaCl,
441 50 mM Tris, pH 8. A 50-mer oligonucleotide consisting of 25 (GT) repeats was added at a final
442 concentration of 5 μM. The protein was then dialyzed against assembly buffer (2M NaCl, 50 mM Tris,
443 150 μM IP6, 5 μM $ZnCl_2$, pH 8) at room temperature in Pierce™ Slide A Lyzer® Mini Dialysis Units
444 (Thermo Fisher Scientific, Waltham, MA). Turbidity measurements at A340 nm were collected in order to
445 quantify the reaction progress by using NanoDrop 1000 Spectrophotometer (Thermo Fisher Scientific,
446 Waltham, MA). Spectrometry readings were collected every 20 min for 2 h, and corrected for any
447 changes in reaction volume due to dialysis.
448 After 2 hours of dialysis, 3 μl of each reaction were spotted onto EMS CF300-CU grids (Ted Pella,
449 Redding, CA) for 2 min. Samples were then blotted with filter paper, washed 3x in deionized water,
450 blotted, and stained in 0.75% (w/v) uranyl formate for 2 min. Samples were imaged by using a FEI
451 Technai Spirit Bio-Twin transmission electron microscope at 120 kV.
452

Acknowledgments

This research was supported by NIH grant R01 AI150468 (to L.M.M.). N.T. was supported by NIH grants T32 DA007097, F32 AI150351, and American Cancer Society Postdoctoral Fellowship PF-21-189-01-MPC. W.G.A. was supported by NIH grant NIH T32 AI083196. TEM was carried out in the Characterization Facility, University of Minnesota, which receives partial support from NSF through the MRSEC and NNCI program.

References

1. **Del Rio C.** 2017. The global HIV epidemic: What the pathologist needs to know. Semin Diagn Pathol **34:**314-317.
2. **Campbell-Yesufu OT, Gandhi RT.** 2011. Update on human immunodeficiency virus (HIV)-2 infection. Clin Infect Dis **52:**780-787.
3. **Nyamweya S, Hegedus A, Jaye A, Rowland-Jones S, Flanagan KL, Macallan DC.** 2013. Comparing HIV-1 and HIV-2 infection: Lessons for viral immunopathogenesis. Rev Med Virol **23:**221-240.
4. **Andersson S, Norrgren H, da Silva Z, Biague A, Bamba S, Kwok S, Christopherson C, Biberfeld G, Albert J.** 2000. Plasma Viral Load in HIV-1 and HIV-2 Singly and Dually Infected Individuals in Guinea-Bissau, West Africa. Arch Intern Med **160:**3286-3293.
5. **de Silva TI, Cotten M, Rowland-Jones SL.** 2008. HIV-2: the forgotten AIDS virus. Trends Microbiol **16:**588-595.
6. **van der Loeff MF, Larke N, Kaye S, Berry N, Ariyoshi K, Alabi A, van Tienen C, Leligdowicz A, Sarge-Njie R, da Silva Z, Jaye A, Ricard D, Vincent T, Jones SR, Aaby P, Jaffar S, Whittle H.** 2010. Undetectable plasma viral load predicts normal survival in HIV-2-infected people in a West African village. Retrovirology **7:**46.
7. **Collaboration H-C, Ray M, Logan R, Sterne JA, Hernandez-Diaz S, Robins JM, Sabin C, Bansi L, van Sighem A, de Wolf F, Costagliola D, Lanoy E, Bucher HC, von Wyl V, Esteve A, Casbona J, del Amo J, Moreno S, Justice A, Goulet J, Lodi S, Phillips A, Seng R, Meyer L, Perez-Hoyos S, Garcia de Olalla P, Hernan MA.** 2010. The effect of combined antiretroviral therapy on the overall mortality of HIV-infected individuals. AIDS **24:**123-137.
8. **Spearman P.** 2016. HIV-1 Gag as an Antiviral Target: Development of Assembly and Maturation Inhibitors. Curr Top Med Chem **16:**1154-1166.
9. **Freed EO.** 2015. HIV-1 assembly, release and maturation. Nat Rev Microbiol **13:**484-496.
10. **Briant L, Gay B, Devaux C, Chazal N.** 2011. HIV-1 Assembly, Release and Maturation. World Journal of AIDS **01:**111-130.
11. **Sundquist WI, Krausslich HG.** 2012. HIV-1 assembly, budding, and maturation. Cold Spring Harb Perspect Med **2:**a006924.
12. **Gheysen D, Jacobs E, de Foresta F, Thiriart C, Francotte M, Thines D, De Wilde M.** 1989. Assembly and Release of HIV-1 Precursor Pr5Wg Virus-like Particles from Recombinant Baculovirus-Infected Insect Cells. Cell **59:**103-112.
13. **Chen B.** 2016. HIV Capsid Assembly, Mechanism, and Structure. Biochemistry **55:**2539-2552.
14. **Molina JM, Segal-Maurer S, Stellbrink HJ, Castagna A, Berhe M, Richmond GJ, Ruane PJ, Sinclair GI, Siripassorn K, Wang H, Patel H, Margot N, Dvory-Sobol H, Hyland RH, Rhee MS, Baeten J, De Jesus E.** 2021. Efficacy and safety of long-acting subcutaneous lenacapavir in phase 2/3 in heavily treatment-experienced people with HIV: week 26 results (Capella study). Journal of the International AIDS Society **24:**75+.
15. **Gottlieb GS, Badiane NM, Hawes SE, Fortes L, Toure M, Ndour CT, Starling AK, Traore F, Sall F, Wong KG, Cherne SL, Anderson DJ, Dye SA, Smith RA, Mullins JI, Kiviat NB, Sow PS, University of Washington-Dakar HIVSG.** 2009. Emergence of multiclass drug-resistance in HIV-2 in antiretroviral-treated individuals in Senegal: implications for HIV-2 treatment in resouce-limited West Africa. Clin Infect Dis **48:**476-483.
16. **Smith RA, Anderson DJ, Pyrak CL, Preston BD, Gottlieb GS.** 2009. Antiretroviral drug resistance in HIV-2: three amino acid changes are sufficient for classwide nucleoside analogue resistance. J Infect Dis **199:**1323-1326.
17. **Maldonado JO, Martin JL, Mueller JD, Zhang W, Mansky LM.** 2014. New insights into retroviral Gag-Gag and Gag-membrane interactions. Front Microbiol **5:**302.
18. **Chukkapalli V, Hogue IB, Boyko V, Hu WS, Ono A.** 2008. Interaction between the human immunodeficiency virus type 1 Gag matrix domain and phosphatidylinositol-(4,5)-bisphosphate is essential for efficient gag membrane binding. J Virol **82:**2405-2417.
19. **Kafaie J, Song R, Abrahamyan L, Mouland AJ, Laughrea M.** 2008. Mapping of nucleocapsid residues important for HIV-1 genomic RNA dimerization and packaging. Virology **375:**592-610.

20. **Grime JMA, Dama JF, Ganser-Pornillos BK, Woodward CL, Jensen GJ, Yeager M, Voth GA.** 2016. Coarse-grained simulation reveals key features of HIV-1 capsid self-assembly. Nat Commun **7:**11568.
21. **Briggs JA, Krausslich HG.** 2011. The molecular architecture of HIV. J Mol Biol **410:**491-500.
22. **Schur FK, Hagen WJ, Rumlova M, Ruml T, Muller B, Krausslich HG, Briggs JA.** 2015. Structure of the immature HIV-1 capsid in intact virus particles at 8.8 A resolution. Nature **517:**505-508.
23. **Zhao G, Perilla JR, Yufenyuy EL, Meng X, Chen B, Ning J, Ahn J, Gronenborn AM, Schulten K, Aiken C, Zhang P.** 2013. Mature HIV-1 capsid structure by cryo-electron microscopy and all-atom molecular dynamics. Nature **497:**643-646.
24. **Gres AT, Kirby KA, KewalRamani VN, Tanner JJ, Pornillos O, Sarafianos SG.** 2015. X-ray crystal structures of native HIV-1 capsid protein reveal conformational variability. Science **349:**99-103.
25. **Pornillos O, Ganser-Pornillos BK, Kelly BN, Hua Y, Whitby FG, Stout CD, Sundquist WI, Hill CP, Yeager M.** 2009. X-ray structures of the hexameric building block of the HIV capsid. Cell **137:**1282-1292.
26. **Pornillos O, Ganser-Pornillos BK, Yeager M.** 2011. Atomic-level modelling of the HIV capsid. Nature **469:**424-427.
27. **Briggs JA, Johnson MC, Simon MN, Fuller SD, Vogt VM.** 2006. Cryo-electron microscopy reveals conserved and divergent features of gag packing in immature particles of Rous sarcoma virus and human immunodeficiency virus. J Mol Biol **355:**157-168.
28. **Qu K, Glass B, Dolezal M, Schur FKM, Murciano B, Rein A, Rumlova M, Ruml T, Krausslich HG, Briggs JAG.** 2018. Structure and architecture of immature and mature murine leukemia virus capsids. Proc Natl Acad Sci U S A **115:**E11751-E11760.
29. **Briggs JA, Riches JD, Glass B, Bartonova V, Zanetti G, Kräusslich HG.** 2009. Structure and assembly of immature HIV. Proc Natl Acad Sci U S A **106:**11090–11095.
30. **von Schwedler UK, Stray KM, Garrus JE, Sundquist WI.** 2003. Functional surfaces of the human immunodeficiency virus type 1 capsid protein. J Virol **77:**5439-5450.
31. **Meng X, Zhao G, Yufenyuy E, Ke D, Ning J, Delucia M, Ahn J, Gronenborn AM, Aiken C, Zhang P.** 2012. Protease cleavage leads to formation of mature trimer interface in HIV-1 capsid. PLoS Pathog **8:**e1002886.
32. **Srinivasakumar N, Hammarskjöld ML, Rekosh D.** 1995. Characterization of deletion mutations in the capsid region of human immunodeficiency virus type 1 that affect particle formation and Gag-Pol precursor incorporation. J Virol **69:**6106-6114.
33. **Doi N, Koma T, Adachi A, Nomaguchi M.** 2019. Role for Gag-CA Interdomain Linker in Primate Lentiviral Replication. Front Microbiol **10:**1831.
34. **Strambio-de-Castillia C, Hunter E.** 1992. Mutational analysis of the major homology region of Mason-Pfizer Monkey Virus by use of saturation mutagenesis. J Virol **66:**7021-7032.
35. **Craven RC, Leure-duPree AE, Weldon RA, Wills JW.** 1995. Genetic analysis of the major homology region of the Rous Sarcoma Virus Gag protein. J Virol **69:**4213-4227.
36. **Ganser-Pornillos BK, von Schwedler UK, Stray KM, Aiken C, Sundquist WI.** 2004. Assembly properties of the human immunodeficiency virus type 1 CA protein. J Virol **78:**2545-2552.
37. **Shoko Nakanishi SW, Naoya Doi, Takaaki Koma, Akio Adachi, Masako Nomaguchi.** 2018. Virological characterization of HIV-1 CA-NTD mutants constructed in a virus-lineage reflected manner. The Journal of Medical Investigation **65:**110-115.
38. **Zhang W, Cao S, Martin JL, Mueller JD, Mansky LM.** 2015. Morphology and ultrastructure of retrovirus particles. AIMS Biophys **2:**343-369.
39. **Martin JL, Cao S, Maldonado JO, Zhang W, Mansky LM.** 2016. Distinct Particle Morphologies Revealed through Comparative Parallel Analyses of Retrovirus-Like Particles. J Virol **90:**8074-8084.
40. **Miyazaki Y, Miyake A, Doi N, Koma T, Uchiyama T, Adachi A, Nomaguchi M.** 2017. Comparison of Biochemical Properties of HIV-1 and HIV-2 Capsid Proteins. Front Microbiol **8:**1082.

41. **Tanaka M, Robinson BA, Chutiraka K, Geary CD, Reed JC, Lingappa JR.** 2016. Mutations of Conserved Residues in the Major Homology Region Arrest Assembling HIV-1 Gag as a Membrane-Targeted Intermediate Containing Genomic RNA and Cellular Proteins. J Virol **90:**1944-1963.
42. **Donna L. Mallery ABK, Nadine Renner, K. M. Rifat Faysal, Mariia Novikova, Leo Kiss, Miranda S. C. Wilson, Bilal Ahsan, Zunlong Ke, John A. G. Briggs, Adolfo Saiardi, Till Böcking, Eric O. Freed, and Leo C. James.** 2021. A stable immature lattice packages IP6 for HIV capsid maturation. Sci Adv **7:**eabe4716.
43. **Rawson JM, Clouser CL, Mansky LM.** 2016. Rapid Determination of HIV-1 Mutant Frequencies and Mutation Spectra Using an mCherry/EGFP Dual-Reporter Viral Vector. Methods Mol Biol **1354:**71-88.
44. **Dostalkova A, Hadravova R, Kaufman F, Krizova I, Skach K, Flegel M, Hrabal R, Ruml T, Rumlova M.** 2019. A simple, high-throughput stabilization assay to test HIV-1 uncoating inhibitors. Sci Rep **9:**17076.
45. **Kucharska I, Ding P, Zadrozny KK, Dick RA, Summers MF, Ganser-Pornillos BK, Pornillos O.** 2020. Biochemical Reconstitution of HIV-1 Assembly and Maturation. J Virol **94**.
46. **Barbie K. Ganser SL, Victor Y. Klishko, John T. Finch, Wesley I. Sundquist.** 1999. Assembly and Analysis of Conical Models for the HIV-1 Core. Science **283:**80-83.
47. **Jiang J, Ablan SD, Derebail S, Hercik K, Soheilian F, Thomas JA, Tang S, Hewlett I, Nagashima K, Gorelick RJ, Freed EO, Levin JG.** 2011. The interdomain linker region of HIV-1 capsid protein is a critical determinant of proper core assembly and stability. Virology **421:**253-265.
48. **Clouser CL, Patterson SE, Mansky LM.** 2010. Exploiting drug repositioning for discovery of a novel HIV combination therapy. J Virol **84:**9301-9309.
49. **Beach LB, Rawson JM, Kim B, Patterson SE, Mansky LM.** 2014. Novel inhibitors of human immunodeficiency virus type 2 infectivity. J Gen Virol **95:**2778-2783.
50. **Heydenreich FM, Miljus T, Jaussi R, Benoit R, Milic D, Veprintsev DB.** 2017. High-throughput mutagenesis using a two-fragment PCR approach. Sci Rep **7:**6787.
51. **Martin JL, Mendonca LM, Marusinec R, Zuczek J, Angert I, Blower RJ, Mueller JD, Perilla JR, Zhang W, Mansky LM.** 2018. Critical Role of the Human T-Cell Leukemia Virus Type 1 Capsid N-Terminal Domain for Gag-Gag Interactions and Virus Particle Assembly. J Virol **92**.
52. **Thompson RF, Walker M, Siebert CA, Muench SP, Ranson NA.** 2016. An introduction to sample preparation and imaging by cryo-electron microscopy for structural biology. Methods **100:**3-15.
53. **Martin JL, Mendonca LM, Angert I, Mueller JD, Zhang W, Mansky LM.** 2017. Disparate Contributions of Human Retrovirus Capsid Subdomains to Gag-Gag Oligomerization, Virus Morphology, and Particle Biogenesis. J Virol **91**.
54. **Studier FW.** 2005. Protein production by auto-induction in high density shaking cultures. Protein Expr Purif **41:**207-234.
55. **Madeira F, Park YM, Lee J, Buso N, Gur T, Madhusoodanan N, Basutkar P, Tivey ARN, Potter SC, Finn RD, Lopez R.** 2019. The EMBL-EBI search and sequence analysis tools APIs in 2019. Nucleic Acids Res **47:**W636-W641.
56. **Price AJ, Marzetta F, Lammers M, Ylinen LM, Schaller T, Wilson SJ, Towers GJ, James LC.** 2009. Active site remodeling switches HIV specificity of antiretroviral TRIMCyp. Nat Struct Mol Biol **16:**1036-1042.
57. **Buchan DWA, Jones DT.** 2019. The PSIPRED Protein Analysis Workbench: 20 years on. Nucleic Acids Res **47:**W402-W407.
58. **Jones DT.** 1999. Protein secondary structure prediction based on position-specific scoring matrices. J Mol Biol **292:**195-202.

Figure 1

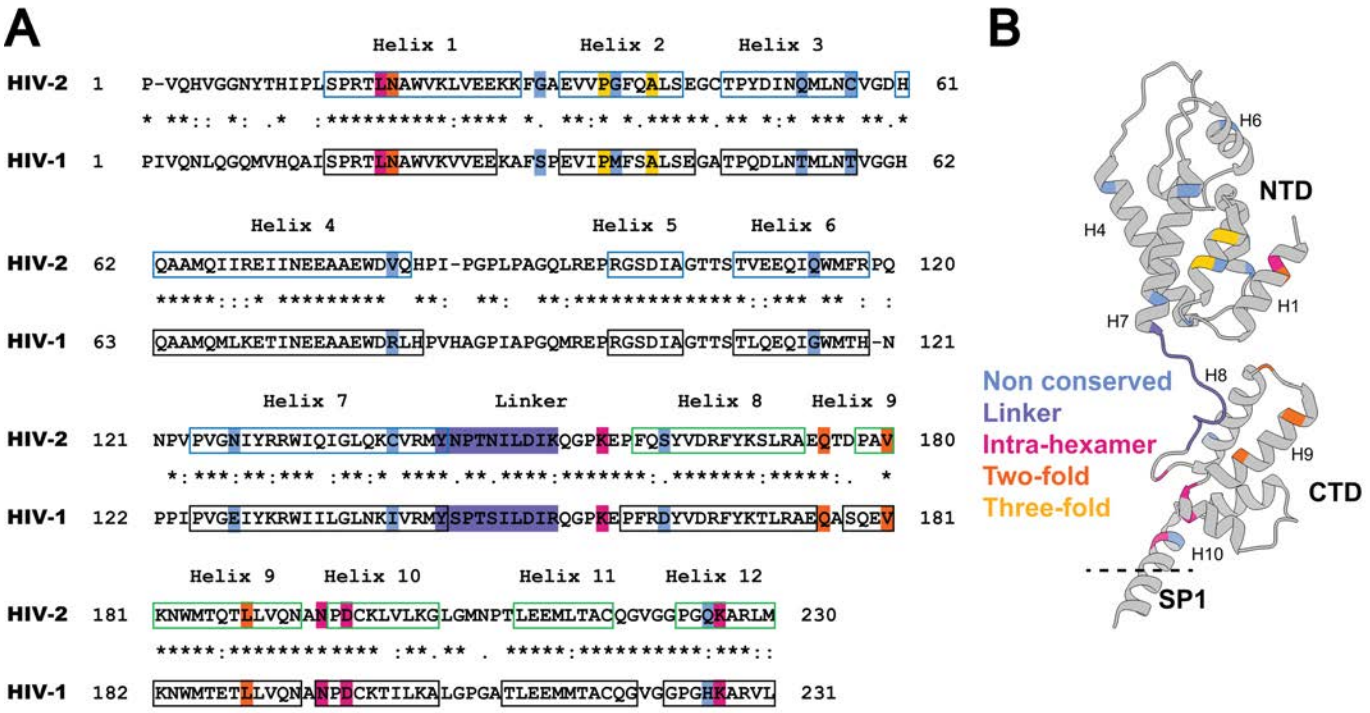

Figure 1. Sequence alignment and CA structure. (A) Alignment of the HIV-1 and HIV-2 CA sequences. Amino acid sequences in CA of HIV-1 NL4-3 (GenBank accession no. AF324493; CA 1-231; Gag 133-363) and HIV-2 ROD (GenBank accession no. M15390; CA 1- 230; Gag 136-365) were aligned by using the Clustal Omega Multiple Sequence Alignment (55). Locations of the HIV-1 immature CA helices in the alignment are based on previous studies (22) (PDB ID: 5L93) and are indicated by black boxes. The HIV-2 immature CA_{NTD} (CA 1-144; Gag 136-279) helices were previously described (56) (PDB ID: 2WLV) and are indicated with blue boxes. The CA_{CTD} (CA 145-230; Gag 280-365) helices are predicted by the PSIPRED server (57, 58), and are indicated by green boxes. "*" indicates conserved amino acids; ":" indicates amino acid substitution with high amino acid similarity; "." indicates amino acid substitutions with low similarity. The blue, purple, magenta, orange, and gold-shaded amino acid residues highlight mutagenesis at non-conserved residues, linker, intra-hexamer interface, two-fold interface, and three-fold interface, respectively. (B) Ribbon diagram of the CA monomer structure. Shown are CA amino-terminal domain (NTD), the carboxy-terminal domain (CTD), the spacer peptide 1 (SP1), and alpha-helices 1, 4, 6,

633 7, 8, 9, and 10 (i.e., H1, H4, H6, H7, H8, H9, and H10). The non-conserved, linker, intra-hexamer, two-

634 fold and three-fold residues analyzed on indicated on the ribbon structure.

635
636

637 **Figure 2**

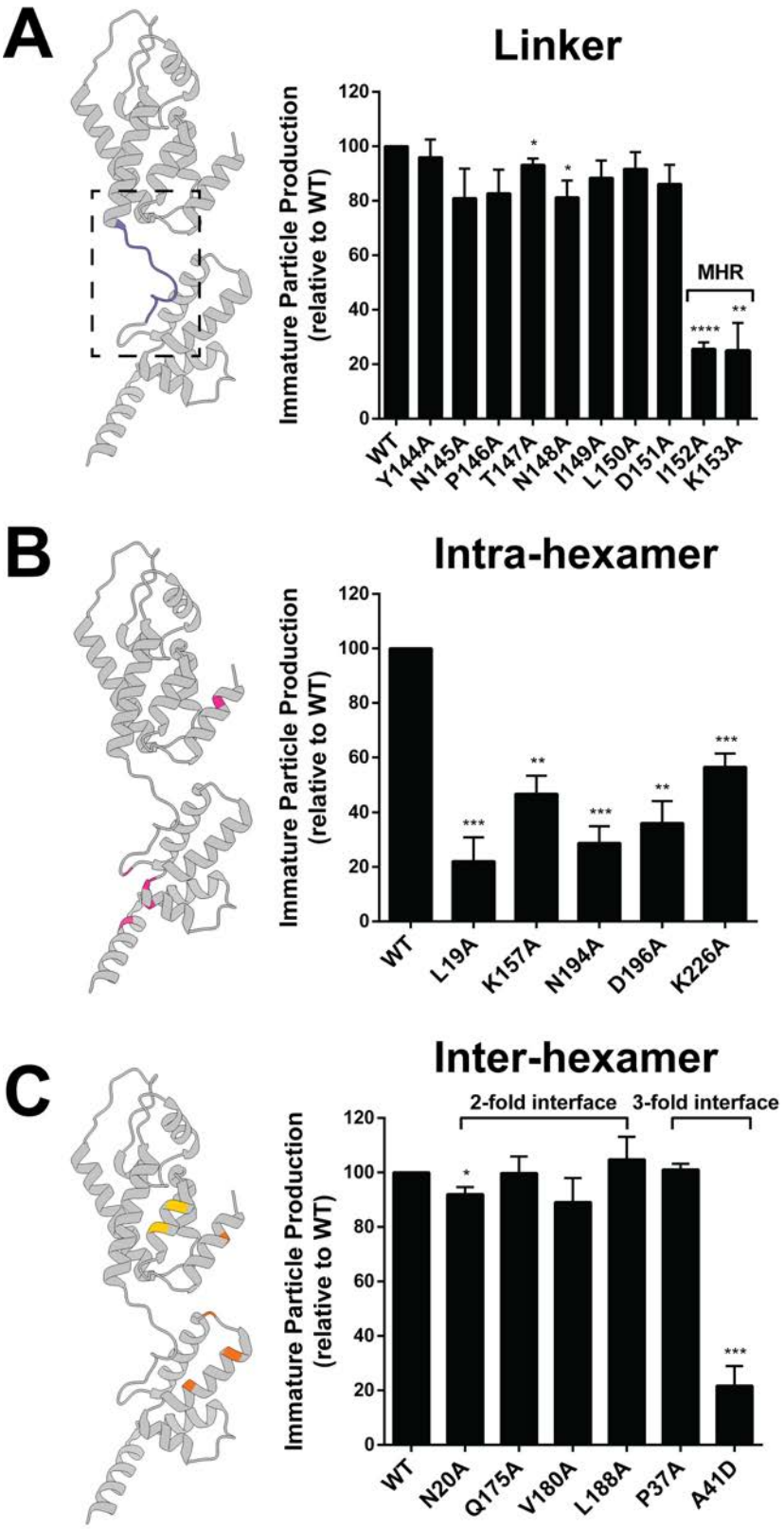

638

639

640 **Figure 2. Immature particle production of HIV-2 CA mutants at the CA_{NTD}-CA_{CTD} linker (A), the**
641 **intra-hexamer interface (B), and the inter-hexamer interface (C).** 293T/17 cells were transfected with
642 Plasmids expressing the HIV-2 Gag (WT or alanine-scanning mutants) were transfected into 293T/17
643 cells, and the cell culture supernatants were harvested 48h post transfection. Immunoblot analysis was
644 conducted to determine the amount of immature particle production for the CA conserved mutants
645 relative to that of WT. Histograms show the relative immature particle production for each HIV-2 CA
646 mutant compared to WT (set to 100). Error bars represent standard error of the mean from three
647 independent experiments. Significance relative to WT was determined by unpaired t test. ****, $P < 0.0001$;
648 ***, $P < 0.001$; **, $P < 0.01$; *, $P < 0.05$. MHR = Major homology region. Mutation locations are colored in
649 the HIV CA monomer structure, using the same color-coding scheme as shown in Figure 1B.
650

651 **Figure 3**

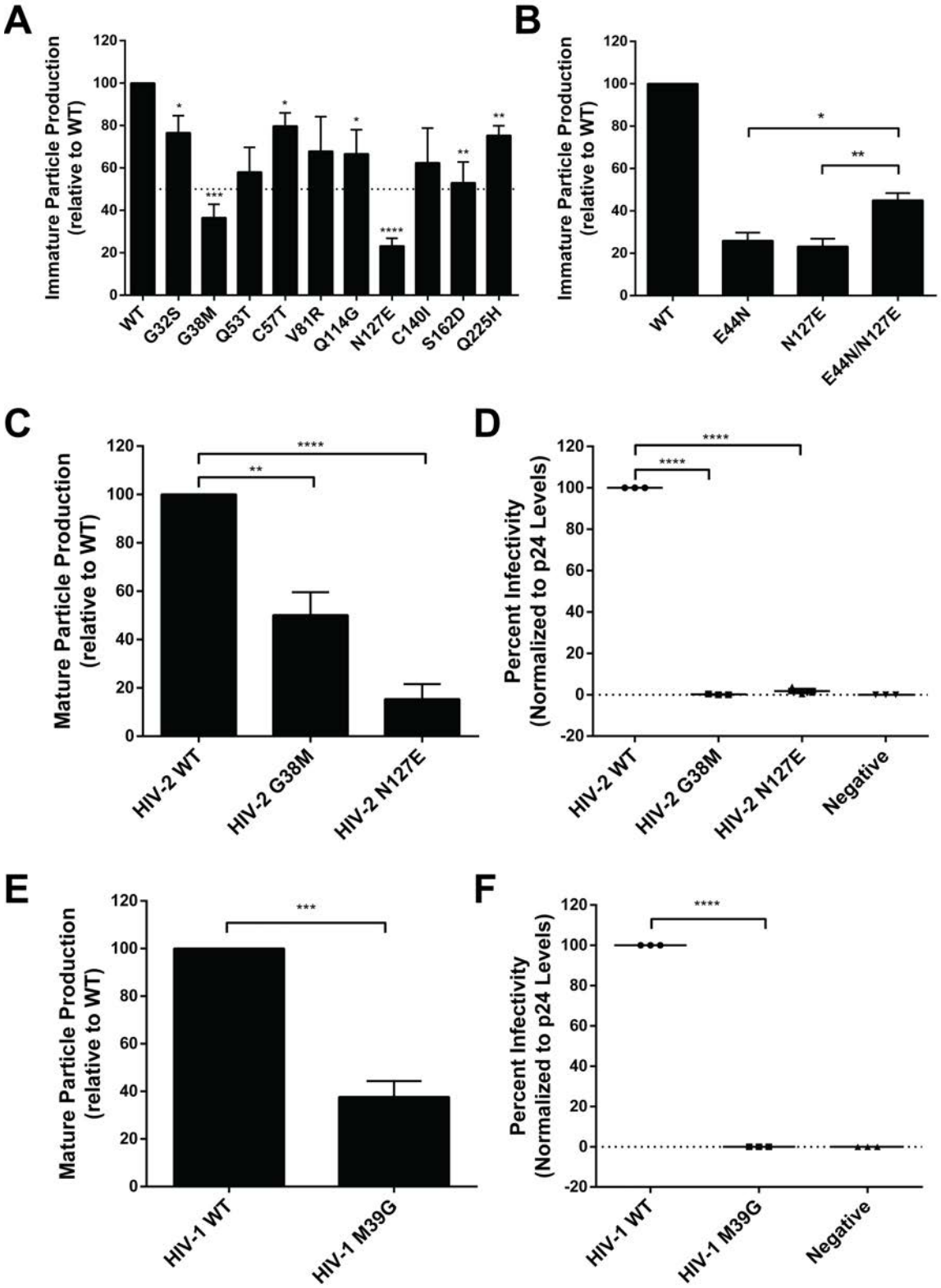

652

653

654 **Figure 3. Particle production and infectivity analysis for HIV CA mutants at non-conserved amino**
655 **acid residues.** (A) Immature particle production of HIV-2 CA mutants at non-conserved amino acid
656 residues. Particle production of mutants from a Gag expression construct is relative to that of WT (set at
657 100). (B) Immature particle production of HIV-2 CA mutants. Shown is particle production of the HIV-2
658 CA E44N, N127E and E44N/N127E mutants relative to that of WT (set at 100). (C) Mature HIV-2 particle
659 production from a HIV-1 single-cycle vector for selected mutants. Shown is particle production of the
660 HIV-2 G38M and N127E CA mutants relative to that of WT (set at 100). (D) Infectivity of HIV-2 CA
661 mutants. Shown is the infectivity relative to that of WT (set at 100) for the HIV-2 G38M and N127E
662 mutants. (E) Mature particle production from a HIV-1 single-cycle vector of a HIV-1 CA mutant. Shown is
663 mature particle production for the HIV-1 M39G CA mutant relative to that of WT (set at 100). (F)
664 Infectivity analysis of HIV-1 CA mutant. Immunoblot analysis of CA p24 levels was conducted to
665 determine the amount of particle production for the M39G mutant relative to that of the WT HIV-1 single-
666 cycle vector. Virus particle infectivity was determined by flow cytometry analysis of infected cells that
667 express a fluorescence reporter gene from the integrated HIV-1 provirus. Mutant particle infectivity was
668 relative to that of the WT HIV-1 vector virus and was normalized to CA p24 levels. Error bars represent
669 standard deviations from three independent experiments. Significance relative to WT was determined by
670 an unpaired t test. ****, $P < 0.0001$; ***, $P < 0.001$; **, $P < 0.01$; *, $P < 0.05$.
671

672 **Figure 4**

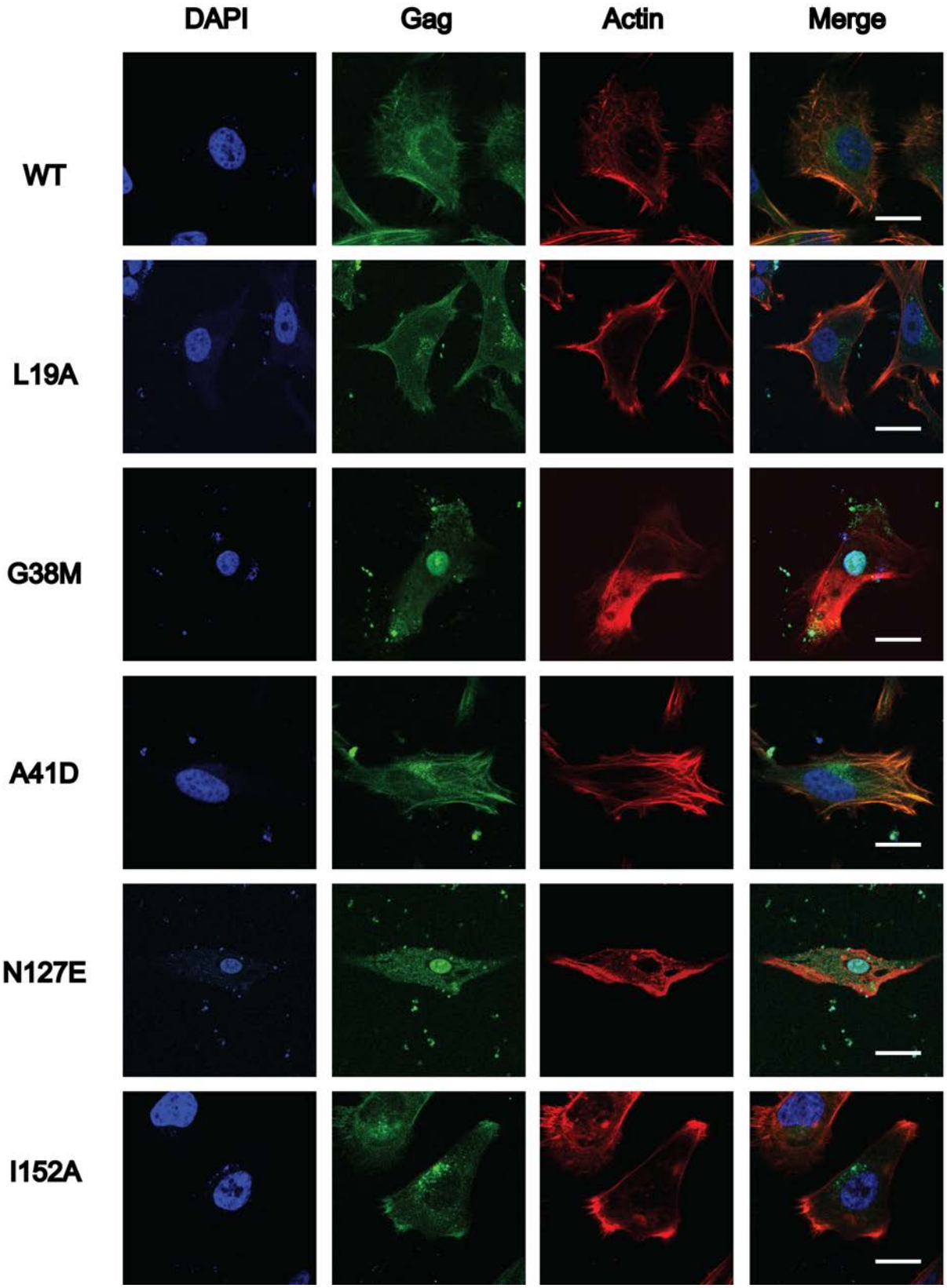

673

674

675 **Figure 4. Subcellular localization of HIV-2 WT Gag and selected CA domain mutants.** HeLa cells
676 were transfected with either HIV-2 Gag-eYFP or a site-directed Gag CA domain mutant. Representative
677 images for WT HIV-2 Gag-eYFP and each Gag CA domain mutant (i.e., L19A, G38M, A41D, N127E and
678 I152A) are shown. At least 15 individual cells were imaged across three independent replicates for a total
679 of 15 cells. Scale bar, 20 μm.
680

681 **Figure 5**

682

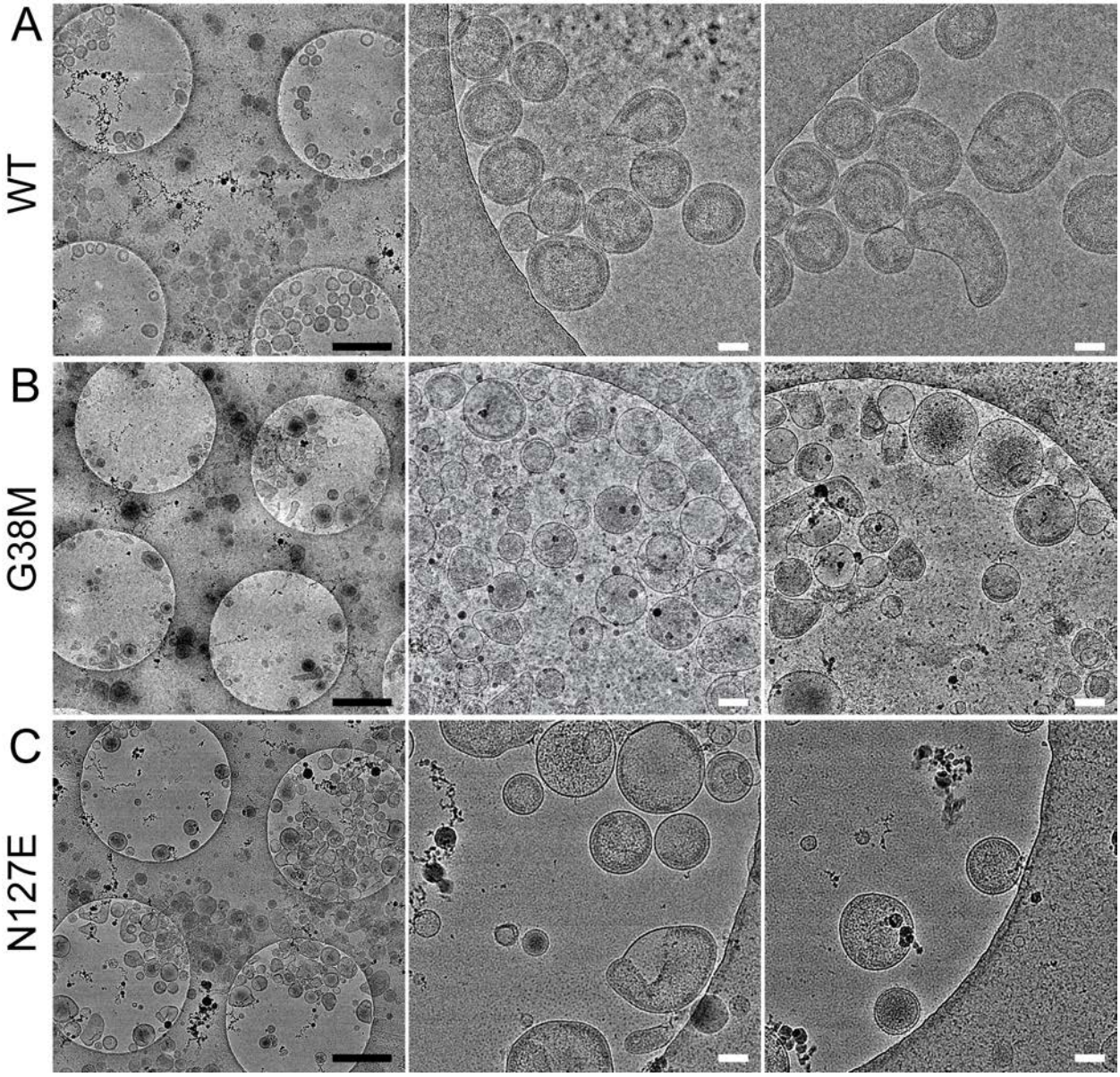

683

684

685 **Figure 5. Cryo-electron microscopy of immature HIV-2 WT or Gag CA domain mutant particles.**

686 The HIV-2 Gag expression plasmid or selected mutant was transfected into 293T/17 cells, and the

687 particles produced from the cells were concentrated and purified from cell culture supernatants prior to

688 cryo-electron microscopy analysis. Representative images are shown for the WT and the G38M and

689 N127E CA domain mutants at two magnifications. At least 200 particles were imaged per virus particle

690 sample. Black scale bars, 1 μm; white scale bars, 100 nm.

691 **Figure 6**

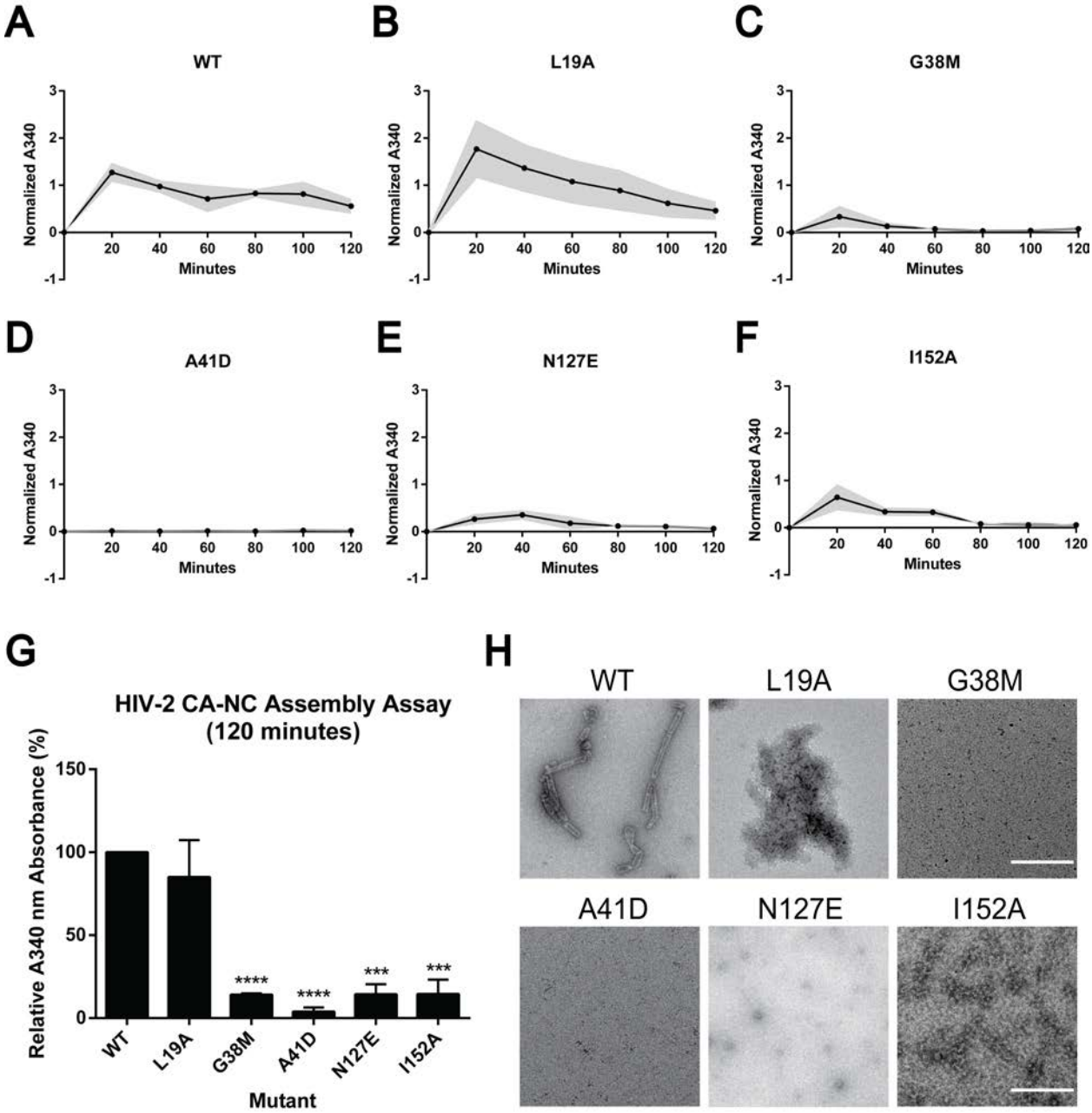

692

693

694

695

696

697

698 **Figure 6. Cell-free assembly of HIV-2 CA-NC protein multimers.** (A-F) Assembly kinetics of HIV-2 WT
699 and the indicated mutants (i.e., L19A, G38M, A41D, N127E, and I152A) were monitored by measuring
700 light scattering at 340 nm while dialyzing the reaction from the sizing buffer into the assembly buffer at
701 the indicated times. Readings were taken every 20 min for 2 h and corrected for any changes in reaction
702 volume due to dialysis. The grey area represents average ± standard error of the mean from three
703 independent experiments. (G) Relative A340 nm absorbance of each HIV-2 CA mutant to WT, sampled
704 at 120 min. Error bars represent the standard error of the mean from three independent experiments.
705 Significance relative to WT was determined by using the unpaired t test. ****, $P < 0.0001$; ***, $P < 0.001$.
706 (H) Negative staining of representative electron microscopy images of HIV-2 CA-NC assembly products,
707 sampled at 120 min. Scale bar, 500 nm.